Existence of a Microporous Corona around the Mesopores of Silica-Based SBA-15 Materials Templated by Triblock Copolymers

M. Impéror-Clerc,[†] P. Davidson,[†] and A. Davidson*[,‡]

Contribution from the Laboratoire de Physique des Solides, UMR 8502-CNRS, Bât. 510, Université Paris-Sud, 91405 Orsay Cedex, France, and Laboratoire de Réactivité de Surface, UMR 7609-CNRS, Université Pierre et Marie Curie, 4 place Jussieu, 75252 Paris Cedex 05, France

Received June 22, 2000

Abstract: Materials showing long-range two-dimensional hexagonal order (called SBA-15 in the literature) were produced by templating a silica precursor (TEOS) with two Pluronic copolymers, $EO_xPO_yEO_x$, of nearly the same x/y (0.3) ratio but different y values ($x = 18$, $y = 60$ and $x = 20$, $y = 70$, respectively). These materials were hydrothermally treated to increase the condensation of silicate species around the Pluronic aggregates and calcined to liberate the hexagonal array of mesopores. All materials, i.e., before and after hydrothermal treatment and calcination, were investigated by X-ray diffraction (XRD), and all calcined samples were further characterized by transmission electron microscopy and N_2 sorption experiments. The large number and narrow width of the XRD powder diffraction lines demonstrate the good crystallographic quality of the materials. This allows us to quantitatively exploit the XRD reflection intensities and to show that simple structural models of the silica lattice cannot account for them. This means that SBA-15 materials cannot be regarded as an ideal hexagonal lattice of pores imbedded in a uniform silica matrix. The structure of the silica walls is more complex and shows a "corona" region of lower density around the cylindrical organic aggregates. This corona becomes microporous upon calcination, and we suggest that it arises from the partial occlusion of the PEO chains in the silica matrix. Modeling the XRD intensities allows us, for all the solids of this series, to derive estimates of pore diameters, corona, and wall thicknesses and to examine the influence on these structural parameters of the hydrothermal treatment.

Introduction

The field of ordered mesoporous materials obtained by solution templating with cationic surfactant molecules has sparked worldwide interest, owing to potential applications for shape-selective heterogeneous catalysis and separation techniques.[1−4] In addition to cationic amphiphiles, neutral block copolymers can also be used as templating agents to produce materials such as the MSU series, which have well-defined pores that are not well-ordered,[5,6] or as SBA-15 compounds, which possess a well-ordered hexagonal array of mesopores.[7−11] This latter development actually represents an important step because catalytic applications of mesoporous solids were somewhat restricted thus far by their low thermal stability in the presence of water due to the thin wall thicknesses (1−1.5 nm, without additional treatment).[12,13] In contrast, the wall thickness of mesoporous solids obtained by block copolymer templating is larger (3−6 nm) and their pore diameter can be more widely varied (3−30 nm for SBA-15 materials compared to 2−10 nm for MCM41 materials).[1,7,8] In this context, it is clear that both pore diameter and wall thickness are key features that need to be tuned in view of the particular application. These features are usually assessed by transmission electron microscopy (TEM) and nitrogen adsorption/desorption isotherms.[1−4,7−11] In practice, both techniques have specific drawbacks. It was recently shown that TEM images depend on the amount of defocus so that the wall thickness estimated in this way can vary by a factor of 2.[14] The results of N_2 sorption isotherms strongly depend on the model that is used to analyze them. The calculation methods based on the Kelvin equation, in particular the method developed by Barrett, Joyner, and Halenda (BJH method),[15] systematically underestimate pore diameters by at least 10%.[9,16−19] In this work,

[†] Université Paris-Sud.

[‡] Université Pierre et Marie Curie.

(1) Kresge, C. T.; Leonowicz, M. E.; Roth, W. J.; Vartuli, J. C.; Beck, J. S. *Nature* **1992**, *359*, 710−712.

(2) Beck, J. S.; Vartuli, J. C.; Roth, W. J.; Leonowicz, M. E.; Kresge, C. T.; Schmitt, K. T.; Chen, C. T.; Olson, D. H.; Sheppard, E. W.; McCullen, S. B.; Higgins, J. B.; Schlenker, J. L. *J. Am. Chem. Soc.* **1992**, *114*, 10834−10843.

(3) Vartuli, J. C.; Schmitt, K. D.; Kresge, C. T.; Roth, W. J.; Leonowicz, M. E.; McCullen, S. B.; Hellring, S. D.; Beck, J. S.; Schlenker, J. L.; Olson, D. H.; Sheppard, E. W. *Chem. Mater.* **1994**, *6*, 2317−2326.

(4) Corma, A. *Chem. Rev.* **1997**, *97*, 2373−2419.

(5) Bagshaw, S. A.; Prouzet, E.; Pinnavaia, T. J. *Science* **1995**, *269*, 1242−1244.

(6) Tanev, P. T.; Pinnavaia T. J. *Science* **1996**, *271*, 1267−1269.

(7) Zhao, D.; Feng, J.; Huo, Q.; Melosh, N.; Fredrickson, G.; Chmelka, B.; Stucky, G. D. *Science* **1998**, *279*, 548−552.

(8) Yang, P.; Zhao, D.; Margolese, D.; Chmelka, B.; Stucky, G. D. *Nature* **1998**, *396*, 152−155.

(9) Luan, Z.; Maes, E. M.; van der Heide, P. W. A.; Zhao, D.; Czernuszewicz, R. S.; Kevan, L. *Chem. Mater.* **1999**, *11*, 3680−3686.

(10) Melosh, N.; Davidson, P.; Chmelka, B. *J. Am. Chem. Soc.* **2000**, *122*, 823−829.

(11) Feng, P.; Bu, X.; Pine, D. *Langmuir* **2000**, *16*, 5304−5310.

(12) Zhao, X. S.; Audsley, F.; Lu, G. Q. *J. Phys. Chem. B* **1998**, *102*, 4143−4146.

(13) Kim, J. M.; Ryoo, R. *Bull. Korean Chem. Soc.* **1996**, *17*, 66−68.

(14) Schacht, S.; Janicke, M.; Schuth, F. *Microporous Mesoporous Mater.* **1998**, *22*, 485−493.

(15) Barrett, E. P.; Joyner, L. G.; Halenda, P. P. *J. Am. Chem. Soc.* **1951**, *73*, 373−380.

(16) Kruk, M.; Jaroniec, M.; Sayari, A. *Chem. Mater.* **1999**, *11*, 492−500.

(17) Lukens, W. W.; Schmidt-Winkel, P.; Zhao, D.; Feng, J.; Stucky, G. D. *Langmuir* **1999**, *15*, 5403−5409.

10.1021/ja002245h CCC: $19.00
Published on Web 11/11/2000

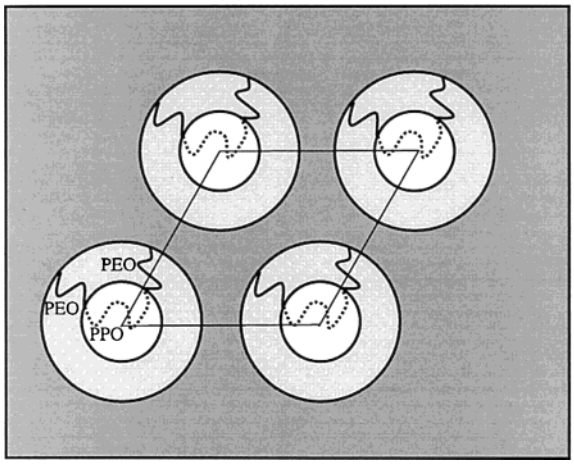

Figure 1. Schematic picture of the organization of uncalcined SBA-15 materials.

we show how X-ray diffraction powder patterns can be quantitatively modeled to obtain lattice parameters, pore diameters, and wall thicknesses. We thus give very detailed new information about the silica organization in the walls of SBA-15 materials.

The mesoporous solids considered here, labeled SBA-15, are synthesized with triblock copolymers and have two-dimensional hexagonal symmetry.[7,8] We used two neutral triblock copolymers (Pluronic (poly(ethylene oxide)−poly(propylene oxide)−poly(ethylene oxide) $EO_{20}PO_{70}EO_{20}$ and $EO_{18}PO_{60}EO_{18}$, BASF®, labeled P123 and P103, respectively) and tetraethyl orthosilicate (TEOS) as the silicate source. At room temperature, the poly(ethylene oxide) (PEO) chains are hydrophilic whereas the poly(propylene oxide) (PPO) chains tend to be hydrophobic, thus driving the formation of direct cylindrical micelles with the PEO chains on the outside. Consequently, a specific and interesting feature of the SBA-15 materials is that, as suggested by NMR,[20] the PEO chains of the Pluronics may be deeply occluded within the silica walls and therefore the density of the walls may not be uniform (Figure 1). Then, the solids obtained upon calcination should display not only the mesoporosity (pore diameter >2 nm) due to the hexagonal arrangement of cylindrical aggregates but also the microporosity (pore diameter <2 nm) liberated by the PEO moieties. This would result in a complex structure in which a microporous silica "corona" surrounds the mesopores. Furthermore, hydrothermal treatments of as-synthesized SBA-15 materials in the reaction solution at different temperatures (80−140 °C) and for different times (11−72 h) are known to increase pore sizes and to decrease wall thicknesses.[7,8,11] Very little information about the evolution of the silica walls introduced by this postsynthesis treatment is currently available.

To our knowledge, previous attempts to model the structure of organized mesoporous solids have only dealt with the MCM-41 materials obtained by templating with cationic surfactants.[14,21−26] The most comprehensive one is the neutron scattering study of White et al., which shows that the mesopores of these materials are not as well-defined as commonly assumed.[23] In contrast, there exists no detailed structural study of SBA-15 materials. We obtained here the dimensions and electron density contrasts of the different parts of the unit cell of these materials by modeling the intensities of their X-ray diffraction powder lines. This information proves that these solids should not be regarded either as an ideal hexagonal lattice of mesopores imbedded in a silica matrix. In particular, we demonstrate here the existence of the microporous corona and we monitor how it is affected by hydrothermal treatments.

Table 1. Main Characteristics of Pluronics and Synthesis Conditions

	Pluronic		synthesis	
	mol wt	formula	Pluronic (wt, g)	temp (°C)
P123	5838	$EO_{20}PO_{70}EO_{20}$	4.0	30
P103	4994	$EO_{17}PO_{60}EO_{17}$	4.4	35

Table 2. Main Characteristics of SBA-15 Materials[a]

solid	*a* (nm)	Si/EO/Cl	D_{BJH} (nm)	V_{mp} (cm^3/g)	V_{MP} (cm^3/g)
P123AU	11.85	1/0.5/0.3			
P123AC	9.6		4.0	0.10	0.60
P123BU	11.9	1/0.4/0.4			
P123BC	11.05		6.0	∗	1.06
P103AU	11.0	1/0.5/0.6			
P103AC	8.8		3.8	0.12	0.52
P103BU	10.85	1/0.4/0.2			
P103BC	10.45		5.0	∗	1.18

[a]Key: *a*, unit cell parameter determined by XRD; Si/EO/Cl molar ratios, ±0.1 error bars; D_{BJH}, pore diameter as obtained on the desorption branch of the isotherm by the BJH formula; V_{mp} and V_{MP}, microporous and mesoporous volumes, respectively; ∗ undetected on β-plot.

Experimental Section

Synthesis. The triblock copolymers were kindly donated by BASF and were used as received. In a typical synthesis, an aqueous solution of Pluronic, acidified to pH 1 by adding HCl, was mixed with TEOS under constant stirring.[7,8] For given amounts of water (6.46 mol), TEOS (0.0409 mol), and HCl (0.24 mol), the amount of Pluronic (4−4.5 g) and the temperature of reaction (30−40 °C) required to obtain a well-ordered SBA-15 material vary, as described in ref 27 (Table 1). The mixture, initially homogeneous, became heterogeneous after less than 15 min of reaction. The heterogeneous mixture was maintained for 24 h at the reaction temperature and then divided into two parts. White solids (labeled A type hereafter) were recovered by filtration of the first part (no washing). The second part was submitted to hydrothermal treatment at 100 °C for 3 days before recovering by filtration other solids, labeled B type in the following. A- and B-type solids were both calcined in air at 400 °C (6 h) in order to remove the Pluronics. Hereafter, calcined solids are respectively labeled AC and BC whereas uncalcined ones are respectively labeled AU and BU. For instance, the material labeled P123BC was templated with the P123 Pluronic, submitted to hydrothermal treatment, and calcined. Uncalcined materials were submitted to chemical analysis at the CNRS Centre d'Analyse-Solaize to obtain the Si/EO/Cl ratios summarized in Table 2. To check for its stability upon air exposure, a given P123BC solid was characterized twice, before and after 6 months of storage in air. To check for its reproducibility, the synthesis at 30 °C of the P123BC solid was performed twice. To check for the effect of the temperature of the synthesis, another P123BC solid was prepared at 35 °C.

(18) Storck, S.; Bretinger, H.; Maier, W. F. *Appl. Catal. A* **1998**, *174*, 137−146.
(19) Sing, K. S. W.; Everett, D. H.; Haul, R. A. W.; Moscow, L.; Pierotti, R. A.; Rouquérol, J.; Siemieniewska, T. *Pure Appl. Chem.* **1985**, *57*, 603−619.
(20) Melosh, N. A.; Lipic, P.; Bates, F. S.; Wudl, F.; Stucky, G. D.; Fredrickson, G. H.; Chmelka, B. F. *Macromolecules* **1999**, *32*, 4332−4342.
(21) Feuston, B. P.; Higgins, J. B. *J. Phys. Chem.* **1994**, *98*, 4459−4462.
(22) Edler, K. J.; White, J. W. *Chem. Mater.* **1997**, *9*, 1226−1233.
(23) Edler, K. J.; Reynolds, P. A.; White, J. W. *J. Phys. Chem. B* **1998**, *102*, 3676−3683.
(24) Stucky, G. D.; Monnier, A.; Schüth, F.; Huo, Q.; Margolese, D.; Kumar, D.; Krishnamurty, M.; Petroff, P.; Firouzi, A.; Janicke, M.; Chmelka, B. F. *Mol. Cryst. Liq. Cryst.* **1994**, *240*, 187−200.
(25) Hammond, W.; Prouzet, E.; Mahanti, S. D.; Pinnavaia, T. J. *Microporous Mesoporous Mater.* **1999**, *27*, 19−25.
(26) Lindén, M.; Blanchard, J.; Schacht, S.; Schunk, S. A.; Schüth, F. *Chem. Mater.* **1999**, *11*, 3002−3008.
(27) Bennadja, Y.; Beaunier, P.; Margolese D.; Davidson, A. *Microporous Mesoporous Mater.*, in press.

Transmission Electron Microscopy. AC- and BC-type solids, as obtained after calcination, were examined by transmission electron microscopy (JEOL JEM-100 CX II microscope operating at 100 kV). The samples were prepared by dispersing the powders as a slurry of acetone which was then deposited and dried on copper grids covered with a holey carbon thin film.

Nitrogen Adsorption/Desorption Isotherms. Nitrogen sorption isotherms at −196 °C were measured on an ASAP 2010 apparatus (Micromeritics, Norcross, GA). Prior to the experiment, the samples were dehydrated at 50 °C overnight and then at ∼120 °C for at least 5 h under a vacuum better than 10^{-4} Torr.

A single-point total pore volume was measured at $P/P^0 = 0.974$. The average diameter of primary mesopores, labeled D_{BJH}, was obtained from the maximum of a pore size distribution calculated using the BJH formula applied to the desorption part of the isotherm for relative (P/P^0) pressures larger than 0.31.[15] The pore size distribution curve exhibits sharp maximums for all samples (fwhm lower than 0.5 nm). Even if such an analysis underestimates pore size, relative variations among samples should be correct.[9,16−19] To assess the possible existence of micropores (diameter <2 nm) in our samples, we have used the β-plot method. As detailed in ref 17, in this method, the volume of nitrogen adsorbed at a given relative pressure P/P^0 is plotted as a function of a β parameter defined as $\beta = \ln(0.4/(P/P^0))^{1/2.7}$.

For clarity, we do not show the curved low-pressure part of the β plot, which is mainly due to adsorption within micropores ($\beta < 0.7$). Then, three different regions can be seen on these plots: (i) a linear region due to multilayer adsorption in mesopores; (ii) a steep region due to capillary condensation within these mesopores; (iii) a last linear region due to multilayer formation onto the external surface of the grains. Microporous, V_{mp}, and mesoporous, V_{Mp}, volumes can be obtained by determining the intercept between the adsorbed amount (y-axis) and the linear segments i and iii. These two extrapolations give V_{mp} and ($V_{mp} + V_{Mp}$), respectively. These volumes, expressed in amounts of nitrogen gas adsorbed at standard temperature and pressure, were multiplied by the coefficient 0.001 547 to be converted into liquid nitrogen volumes, as adsorbed at −196 °C.

X-ray Diffraction. Compared to MCM-41 materials, the rather large values of the hexagonal lattice parameters (∼10 nm) of the materials investigated here make it necessary to record X-ray diffraction lines at rather low scattering angles, as described below. Such X-ray scattering experiments were performed first with an already described laboratory setup[28] and second at the D43 experimental station of the LURE synchrotron facility (Orsay, France).[29] In the following, we only show results obtained at LURE although similar results were obtained with the laboratory rotating anode setup, with a lower resolution. The D43 experimental station uses a single bent Ge monochromator (111 reflection) to select the wavelength ($\lambda = 0.145$ nm) and to focus the beam. The beam size was defined by a collimator of 0.5 mm diameter. Vacuum flight tubes were inserted between the sample and the detection in order to get rid of the parasitic air scattering. Powder samples were held in Lindemann glass capillaries usually of 1 mm diameter. Scattering patterns were recorded on phosphor image plates scanned with a pixel size of 0.1 × 0.1 mm^2. The sample−detection distance was precisely determined by calibration with silver behenate ($d_{001} = 5.838$ nm). The diffraction patterns consisted in several concentric circles so that the scattered intensity was azimuthally integrated and plotted as a function of the scattering angle 2θ. These curves are called "powder scans" in the following.

The scattering of the calcined samples, due to the large contrast between silica and the empty pores, is naturally much stronger than that of the uncalcined ones. Exposure times typically ranged from a few minutes for calcined samples up to 2 h for uncalcined ones.

Additional high-resolution experiments were performed at the H10 experimental station of LURE. This apparatus, already described in detail,[30] involves a diffractometer which allows one to perform scans of the powder diffraction lines with a resolution of $\Delta q \approx 0.014$ nm^{-1}, where q is the scattering vector modulus $q = (4\pi \sin\theta)/\lambda$. Thus, any line broadening due to grain size smaller than ∼900 nm can be detected.

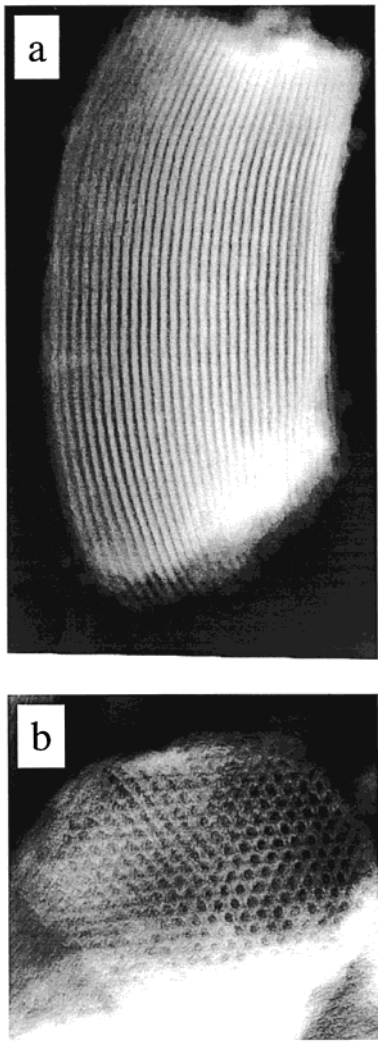

Figure 2. Transmission electron microscopy images of the P123BC solid. Electron beam perpendicular (a) and parallel (b) to the main axis of the pores (grain length ∼1 μm).

Results

Electron Microscopy. SBA-15 powder grains are in the shape of curved cylinders of relatively uniform size (typically 200−400 nm diameter and 1−3 μm long). As illustrated in Figure 2 for the P123BC sample, a well-ordered hexagonal array of mesopores is observed for all calcined samples, when the electron beam is parallel to the main axis of these cylinders. When the electron beam is perpendicular to the main axis, the hexagonal arrays of cylindrical pores are viewed from the side, resulting in a striped image. The two-dimensional hexagonal structure (p6mm) is therefore confirmed. According to typical TEM images, one can roughly estimate the pore diameter to 3−6 nm and the lattice parameter to ∼10 nm.

Nitrogen Adsorption/Desorption Isotherms. The nitrogen sorption isotherms of SBA-15 materials have been used to obtain information about their mesoporosity. These isotherms are of type IV, according to the IUPAC classification.[19] As illustrated in Figure 3a for the P123AC and P123BC solids, a sharp increase of the adsorbed N_2 volume, characteristic of the capillary condensation within mesopores, occurs for a relative pressure P/P^0 larger than 0.4. This jump is irreversible: a hysteresis loop with parallel desorption and adsorption branches is observed (type H1). The sharpness of this jump indicates the

(28) Impéror-Clerc, M.; Davidson, P. *Eur. Phys. J. B* **1999**, *9*, 93−104.

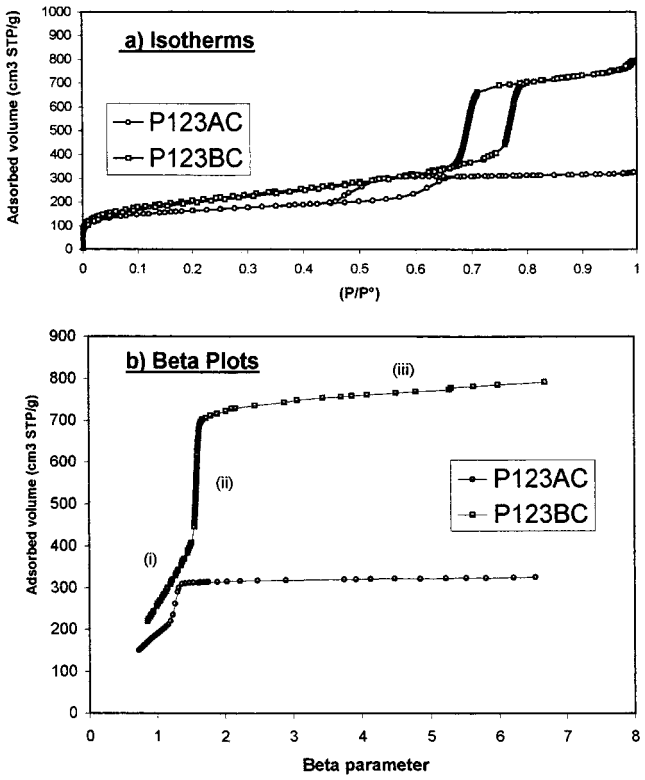

Figure 3. N_2 adsorption/desorption experiments with the P123AC and P123BC samples: (a) isotherms at 77 K; (b) β plots, $\beta = \ln(0.4/(P/P^0))^{1/2.7}$.

uniformity of mesopore sizes. Nitrogen condensation occurs at relative pressures much lower for the AC-type solids than for the BC-type ones. This indicates that the hydrothermal treatment induces a significant mesopore enlargement, as confirmed by BJH analysis (Table 2). Similarly, for BC-type solids, nitrogen condensation occurs at much higher relative pressure for the solids based on P123 than for the ones based on P103, thus suggesting that the solids templated with P123 have larger pores. Furthermore, the BC-type solids have Brunauer−Emmett−Teller (BET) surface areas and overall pore volumes similar to the values previously reported in the literature (for instance, $S_{BET} = 841$ m^2/g and $V_{0.974} = 1.11$ mL/g).[7−9]

These isotherms have been further used to evidence an additional microporosity. The β plots (Figure 3b) of AC-type solids systematically yield nonzero V_{mp} values, thus indicating the presence of micropores. In contrast, this microporosity could not be detected in the BC-type samples.

X-ray Diffraction. Powder X-ray diffraction patterns were obtained for all solids, calcined and uncalcined. The powder scans derived from the powder patterns are shown in Figure 4a,b. The first five diffraction lines (10), (11), (20), (21), and (30) are observed for most samples. Moreover, the patterns of the A-type solids also display weak (22) and (31) diffraction lines. The relatively large number of observable reflections and the fact that their widths remain limited by the resolution of the D43 experimental station demonstrate the good quality of the long-range order. In this respect, the solids described here compare favorably with the best ordered mesoporous materials of hexagonal symmetry reported in the literature.[23] Nevertheless, the limited number of observable diffraction lines suggests that the two-dimensional (2-d) lattice is not perfect. More precisely, the intensities of the diffraction lines decrease rapidly with their order even though their widths are resolution limited. This situation often arises with lyotropic hexagonal mesophases.[28,31] This is due both to the form factor of the cylinders and to the existence of an appreciable disorder similar to frozen thermal fluctuations,[32] the effect of which may be described by a Debye−Waller factor. This point will be dealt with in more detail under Structural Models.

In addition, a continuous background, which slowly decreases with scattering angle, is also observed, especially for calcined samples, and hampers the measurement of weak diffraction lines. This background approximately follows a q^{-3} decay and might therefore be interpreted as the "Porod" regime of the small-angle scattering signal arising from rough interfaces.[33,34] Due to a better contrast, this background would then be larger for calcined samples. In this work, we only focus on the diffraction line intensities and do not analyze this background any further since it is not relevant to our approach.

All the diffraction lines of the scattering patterns could be accurately indexed with a 2-d hexagonal lattice. The lattice constants a of each solid are given in Table 2. Error bars on these values are ∼0.5%. As already reported in the literature,[7,8,11,27] calcination brings about a contraction of the 2-d lattice due to further condensation of the silica network. Moreover, it is clear that the A-type solids undergo a much larger contraction (∼20%) than the B types (∼3−8%).[11,27]

Using the higher resolution H10 experimental station, the powder diffraction scan of the P103BC solid actually shows that the diffraction lines are not resolution limited (Figure 5). By applying Scherrer's formula,[32] a transverse grain size of 370 nm is obtained, in good agreement with the electron microscopy measurements. This proves that the hexagonal long-range order actually extends over the whole grain (∼35 unit cells), which can be considered as a single domain, thus confirming the good crystallographic quality of the samples. Moreover, the domain size is large enough not to affect the diffraction lines of the powder scans performed at the D43 experimental station, which is a lower resolution setup. However, the limited domain size may bring about the continuous background mentioned above.[23]

Close inspection of the powder scans reveals that, for all the A-type solids, the intensity of the (11) diffraction line is weaker than that of the (20). In contrast, none of the B-type solids display this intensity inversion. Structural information can be obtained from this intensity inversion by modeling the structure factor of the unit cell as described in the next section. The peak integrated intensities were measured from the powder scans by determining the area of each peak and subtracting the contribution due to the background. The intensities of the (*hk*) diffraction lines normalized to that of the (10) reflection are shown for each solid in Table 3. The (22) and (31) diffraction lines could not be fully resolved so their intensities were estimated together. The error bars on these values are ∼10% and are essentially due to background subtraction. Less than 1% variation on the lattice constant a and less than 10% variation on the relative intensities of the (10) and (11) diffraction lines are obtained with the calcined P123BC solid after six months of air exposure.

(29) Pelta, J.; Durand, D.; Doucet, J.; Livolant, F. *Biophys. J.* **1996**, *71*, 48−63.

(30) Gailhanou, M.; Dubuisson, J. M.; Ribbens, M.; Roussier, L.; Bétaille, D.; Créoff, C.; Lemonnier, M.; Denoyer, J.; Jucha, A.; Lena, A.; Idir, M.; Bessière, M.; Thiaudière, D.; Hennet, L.; Landron, C.; Coutures, J. P. Submitted to *Nucl. Instrum. Methods Sect. A.*

(31) Alexandridis, P.; Olsson, U.; Lindmann, B. *Langmuir* **1998**, *14*, 2627−2638.

(32) Guinier, A. *X-ray Diffraction in Crystals, Imperfect Crystals and Amorphous Bodies*; Dover: New York, 1994.

(33) Guinier, A.; Fournet, G. *Small Angle Scattering of X-rays*; John Wiley & Sons: New York, 1955.

(34) Pauly, T. R.; Liu, Y.; Pinnavaia, T. J.; Billinge, S. J. L.; Rieker, T. P. *J. Am. Chem. Soc.* **1999**, *121*, 8835−8842.

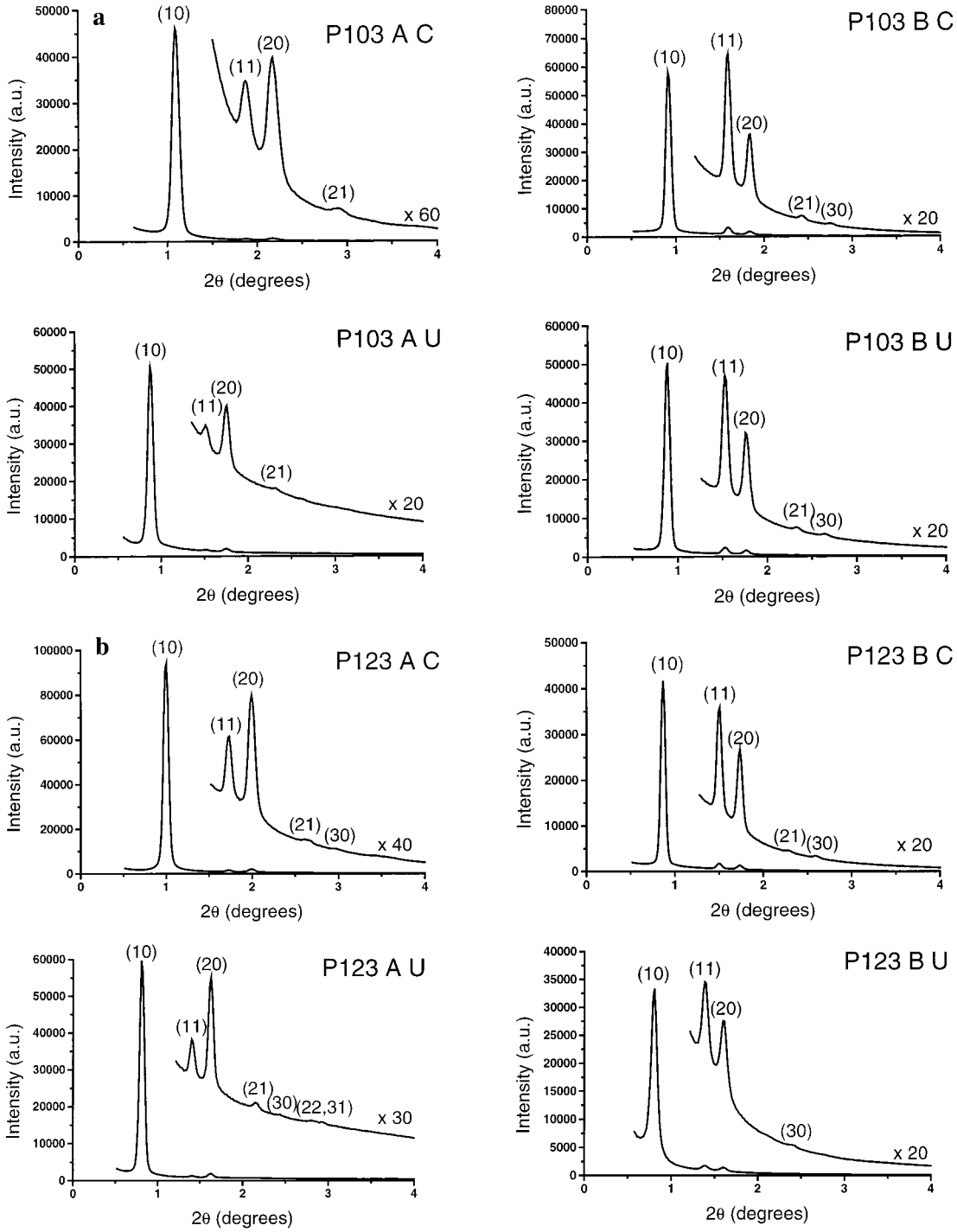

Figure 4. X-ray diffraction powder scans of the SBA-15 materials. (a) Templated with the P103 Pluronic. Uncalcined: P103AU and P103BU. Calcined: P103AC and P103BC. (b) Templated with the P123 Pluronic. Uncalcined: P123AU and P123BU. Calcined: P123AC and P123BC.

Similar results are obtained with two distinct P123BC samples synthesized at 30 °C (∼2% variation on the lattice constant *a* and less than 10% variation on the relative intensities of the (10) and (11) diffraction lines). Finally, increasing the temperature of synthesis (35 °C) yields a significant decrease of the lattice constant *a* (∼7%) and a more than 10% variation in the relative intensities of the (10) and (11) diffraction lines.

The comparison of Figure 4a and b shows that the materials based on P123 have powder scans quite similar to the respective ones of the materials based on P103. This remark suggests that the same description of the unit cell may apply quantitatively for both families of materials.

Structural Models

In this section, we try to analyze the diffraction intensities of all the A-type and B-type solids in the framework of various structural models of the hexagonal unit cell. The different parameters of these models are the dimensions and electron densities of each area (silica walls, Pluronic, mesopores) of the unit cell. Let us emphasize here two points. First, the scattering power only depends on the electron density contrast between the different moieties of the unit cell. This means that the electron density levels are only obtained up to an additive constant. However, for the calcined samples, we can set the electron density value of the mesopores to zero. Second, we

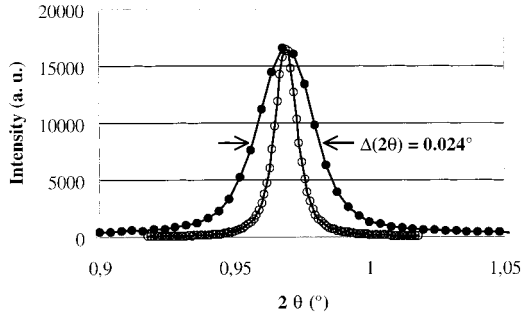

Figure 5. High-resolution profile of the (10) diffraction line of the P103BC solid. The thin line shows the direct beam profile, which determines the experimental resolution.

have not performed absolute measurements of the diffraction intensities so that, for any given solid, the intensities of the various (*hk*) diffraction lines are only given relative to that of the (10) line. This means that the electron density levels are only considered through their ratios. In the following subsections, we only illustrate the differences between various models on the structure of the P123 BC solid because all solids behave in the same way in this respect. However, in the end of this section, we show, for all solids, the results provided by the best models.

For all models, we calculate the diffraction intensities in the following form:

$$I(\bar{q}) = KM(h,k)\frac{|A(\bar{q})|^2}{\bar{q}^2}$$

where

$$\bar{q} = qa = \frac{4\pi}{\sqrt{3}}\sqrt{h^2 + k^2 + hk}$$

is the normalized scattering vector modulus, $M(h,k)$ is the line multiplicity, $1/\bar{q}^2$ represents the Lorentz factor for a powder, and $A(\bar{q})$ is the form factor introduced by each model (Fourier transform of the electron density distribution in the unit cell). K is a multiplicative constant adjusted to normalize the intensity of the (10) line to the arbitrary value of 10 000.

Model Based on Two Density Levels. The simplest model of a SBA-15 material is a 2-d hexagonal assembly of cylinders imbedded in a uniform silica matrix (Figure 6a). Let us call r the radius of the cylinders, d_1 their electron density, and d_2 the electron density of the silica matrix. We use a normalized radius defined by $\bar{r} = r/a$. In the frame of this model, the amplitudes of the diffraction lines are given by the formula

$$A(\bar{q}) = (d_2 - d_1)2\pi a^2\bar{r}^2\frac{J_1(\bar{q}\bar{r})}{\bar{q}\bar{r}}$$

where J_1 is the Bessel function of order 1.[35] The only fit parameter of this model is $\bar{r}$ because d_1 and d_2 only enter in the prefactor, which is normalized. The fit of the diffraction data by this model is shown in Table 4. It is obvious that this intuitive model does not describe the data properly and is therefore inadequate. It predicts much too large intensities for the higher order reflections (21) and (30). Moreover, it predicts intensity inversions between the (11) and (20) reflections for the P123BC and P123BU solids. This behavior strongly suggests the need to introduce more complicated models.

(35) Oster, G.; Riley, D. P. *Acta Crystallogr.* **1952**, *5*, 272−276.

Model Based on Two Density Levels and a Debye−Waller Factor. We now consider that the positions of the cylinders may fluctuate in the unit cell, for instance, due to thermal fluctuations frozen in by silica polymerization (Figure 6b). This simply affects the diffraction intensities through a Debye−Waller exponential factor so that the diffraction amplitudes now read

$$A(\bar{q}) = (d_2 - d_1)2\pi a^2\bar{r}^2\frac{J_1(\bar{q}\bar{r})}{\bar{q}\bar{r}}\exp\left(-\frac{\langle\bar{u}^2\rangle\bar{q}^2}{4}\right)$$

where $\langle\bar{u}^2\rangle$ is the normalized mean-squared displacement of the cylinders. This model involves two fit parameters $\bar{r}$ and $\langle\bar{u}^2\rangle$. As expected (see Table 4), the intensities of the higher order reflections are now greatly reduced and the description of the data looks much more satisfactory. The values of $\langle\bar{u}^2\rangle$ obtained correspond to average displacements of the order of 1 nm, i.e., ∼10% of the unit cell parameter. This model provides a better fit to the data (Table 4), but it predicts for all calcined samples, mesopore diameters that are much too large compared to the values derived from N_2 adsorption/desorption experiments and TEM. For the P123 BC solid for instance, N_2 adsorption gives a mesopore diameter of 6 nm, a value that is known to be underestimated by ∼10%.[9,16−19] The model predicts a mesopore diameter of 8.2 nm, clearly conflicting with this estimate. Therefore, although this model is more efficient than the previous one, it is still not satisfactory.

Model Involving a Corona of Uniform Density. A more realistic model should distinguish the regions of dense silica from the regions (corona) where silica species and ethylene oxide segments are mixed in uncalcined materials (Figure 1). These latter regions are microporous in the calcined solids. In this section and the next one, we consider two variants of models that involve a corona. First, we consider a model (Figure 6c) in which the cylinders have an inner core of density d_1 and radius r_1 and are surrounded by a corona of uniform density d_2 and of radius r_2. The density of the continuous silicate matrix is labeled d_3. The densities affect the intensities only through the ratio $\alpha = (d_2 - d_1)/(d_3 - d_1)$ so that this model has three fit parameters (α, $\bar{r}_1$, $\bar{r}_2$). The diffraction amplitudes now read

$$A(\bar{q}) = (d_3 - d_1)2\pi a^2\left[\alpha\bar{r}_1^2\frac{J_1(\bar{q}\bar{r}_1)}{\bar{q}\bar{r}_1} + (1-\alpha)\bar{r}_2^2\frac{J_1(\bar{q}\bar{r}_2)}{\bar{q}\bar{r}_2}\right]$$

This model gives a quite satisfactory description of the diffraction data (see Table 4) with mesopore diameters in better agreement with the other characterization techniques. Including a Debye−Waller factor may result in an even better agreement but would unnecessarily increase the number of fit parameters.

Model Involving a Corona of Linearly Increasing Density. Another way of introducing a corona is to consider a constant gradient of silica density between the mesopores and the denser part of the walls (Figure 6d). The advantage of this model compared to the previous one, is that it only has two fit parameters ($\bar{r}_1$, $\bar{r}_2$). In this frame, the diffraction amplitudes can be expressed as

$$A(\bar{q}) = \frac{(d_3 - d_1)2\pi a^2}{\bar{r}_2 - \bar{r}_1}\left[\bar{r}_1^3\left(\frac{J_1(\bar{q}\bar{r}_1)}{\bar{q}\bar{r}_1} - \mathrm{int}(\bar{q}\bar{r}_1)\right) - \bar{r}_2^3\left(\frac{J_1(\bar{q}\bar{r}_2)}{\bar{q}\bar{r}_2} - \mathrm{int}(\bar{q}\bar{r}_2)\right)\right]$$

where

Table 3. Intensities of the (*hk*) Diffraction Lines Normalized to That of the (10) Line for Each A-Type and B-Type Solid

	P103AC	P103BC	P103AU	P103BU	P123AC	P123BC	P123AU	P123BU
(10)	10000	10000	10000	10000	10000	10000	10000	10000
(11)	38	434	34	324	79	289	56	283
(20)	107	203	148	213	165	214	181	240
(21)	6	11	5	6	4	2	9	
(30)		5		6	1	5	1	2
(22)	1		0.5		3		6	
(31)								

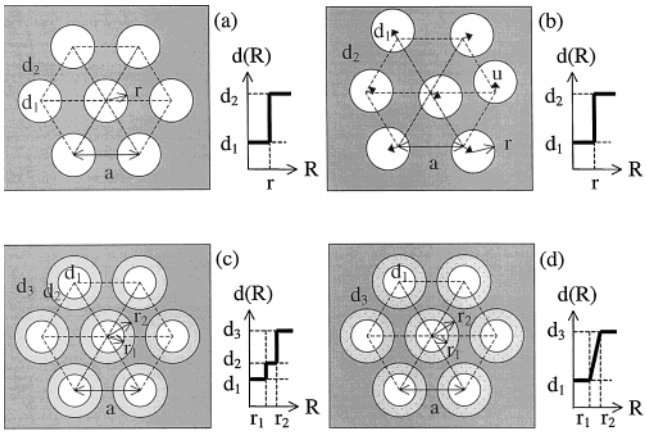

Figure 6. Schematic representations of the structure in the frame of different models based on (a) two density levels and (b) two density levels and a Debye−Waller factor. Arrows indicate a random displacement of the pore centers. (c) A corona of uniform density. (d) A corona of linearly increasing density.

$$\mathrm{int}(\bar{q}\bar{r}) = \frac{1}{3}{}_1F_2\left[\left\{\frac{3}{2}\right\},\left\{1,\frac{5}{2}\right\}, -\frac{(\bar{q}\bar{r})^2}{4}\right]$$

involves a hypergeometric function.[36,37]

The results for the P123BC solid (Table 4) are almost as good as those of the previous one. Most importantly, this model, which has the same number of fit parameters as the model based on two density levels considered in the section Model Based on Two Density Levels and a Debye−Waller Factor, always provides better fits of the data and yields pore radii in much better agreement with the nitrogen sorption experiments.

Figure 7, which summarizes the density profiles of the different models for the P123BC solid, shows that this model and the previous one yield similar radii for the different parts of the unit cell. Therefore, both models are comparable and provide two limit descriptions of the corona density profiles. The results of these two models are discussed in more detail from the chemical point of view in the Discussion.

Discussion

Let us first analyze the information provided by the structural models. The failure of the simple model based on two density levels to properly describe the diffraction data of the SBA-15 materials shows that these solids cannot be regarded as an ideal array of mesopores. Considering a Debye−Waller factor does not really improve things since the pore diameters modeled in this way show too large discrepancies with estimates obtained from N_2 sorption experiments (Figure 3). This means that the structure of SBA-15 materials is more complex, which substantiates the assumption of the existence of two silica density regions around the cylinders. A somewhat similar situation was pointed out by White et al. for MCM-41 materials.[23] However, for these latter materials, the wall region of lower silica density (called lining) arises from the meandering of smooth tubes. This explanation does not hold here because a microporosity is indeed observed for the AC-type solids and because the templating agents are very different from the cationic surfactants used in MCM41 syntheses. The corona region can be taken into account by introducing either a third level of silica density (Figure 6c) or a linear density variation between the mesopore and the wall (Figure 6d). Considering the different numbers of model parameters (respectively, 3 and 2) and experimental error bars, both models provide similarly good descriptions of the data. For all the solids synthesized, we detail in Table 5 the fits obtained with the two models involving a corona. These results suggest the following comments:

(i) For calcined samples, the uniform corona model directly gives the ratio of the corona silica density to that of the denser part of the walls, d_2/d_3. For instance, for the P123 AC solid, the corona has a density of ∼33% that of the denser part of the walls, which we may assume to be that of amorphous silica.[23] This implies that, at least in this case, the corona has a very large volume fraction of pores. Unfortunately, for uncalcined samples, we cannot set the electron density of the cylinders to zero, and since we did not perform diffraction intensity absolute measurements, estimating the silica density of the corona is awkward.

(ii) As expected, the solids based on P123 and the respective ones based on P103 have very similar organizations. Even though they have different lattice parameters a and pore sizes r_1, the ratio r_1/a does not depend on the choice of one of these two Pluronics. This directly appears in their relative diffraction intensities (Table 3) and consequently also in their structures as obtained from the models. This obviously results from the fact that P123 and P103 have almost the same hydrophilic/hydrophobic ratio and in a way validates the idea that one can tune the organization of silica by tailoring this Pluronic specific feature.

(iii) Calcination has distinct effects depending on whether the solids have undergone thermal treatment (A or B type). The lattice parameter of A-type solids contract by a large extent (∼20%). Moreover, while the r_2/a ratio remains almost constant, the r_1/a ratio strongly increases. In absolute values, the thickness ($r_2 - r_1$) actually decreases, demonstrating that the microporous corona of the A-type solids contracts upon calcination. In contrast, B-type solids contract slightly and uniformly upon calcination (3−8%), thus keeping their r_1/a and r_2/a ratios almost constant. Finally, it is important to stress that the presence of micropores in SBA-15 materials has been recently confirmed by platinum and carbon deposition followed by dissolution of the silica framework.[38,39]

(36) *Handbook of Mathematical Functions*; Abramowitz, M., Stegun, I. A., Eds.; Dover Publications Inc.; New York, 1972; Chapter 15.

(37) All fitting procedures were performed with the Mathematica 4.0 software, Wolfram Research Inc. (http://www.wolfram.com).

(38) Kruk, M.; Jaroniec, M.; Ko, C. H.; Ryoo, R. *Chem. Mater.* **2000**, *12*, 1961−1968.

(39) Jun, S.; Joo, S. H.; Ryoo, R.; Kruk, M.; Jaroniec, M.; Liu, Z.; Oshuna, T.; Terasaki, O. *J. Am. Chem. Soc.* **2000**, *43*, 10712−10713.

Table 4. Fits of the Experimental Diffraction Intensities for the P123 BC Solid from the Four Different Structural Models (Described in the Text)

	P123 BC type				
(*hk*)	*I* obsd	*I* 2-d levels	*I* 2-d levels + Debye−Waller	*I* uniform corona	I increasing density corona
r (nm)		3.9	4.1	3.5, 4.7	2.9, 5.2
$\bar{r} = r/a$		0.355	0.372	0.317, 0.429	0.266, 0.467
			$\sqrt{u^2} = 0.95$ nm	$d_2/d_3 = 0.55$	
χ^2		13753	11	0.6	4
(10)	10000	10000	10000	10000	10000
(11)	289	241	289	289	289
(20)	214	320	214	214	214
(21)	2	6	1	0	1
(30)	5	19	8	5	7
(22)	0	20	2	1	1
(31)		21	1	0	0

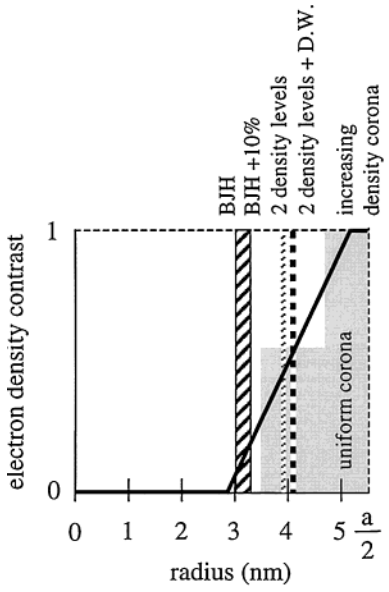

Figure 7. Electron density profiles provided by the different models.

Let us now analyze the results from a more chemical point of view. Our experiments clearly show that the most relevant feature of all these solids lies in whether they have undergone hydrothermal treatment. Thus, all A-type solids show the intensity inversion between the (11) and (20) powder diffraction lines whereas this inversion is not observed for any B-type solid. The polymerization degree of silica is obviously increased by the hydrothermal treatment, thus limiting the calcination-induced contraction of the unit cell. The comparison of the ratios d_2/d_3 (Table 5) shows that the coronas of the B-type solids also have larger densities than those of the A-type ones, which may explain why no microporosity could be detected with the B-type solids. In addition, as already concluded by Stucky et al.,[7,8] the B-type solids have larger pore diameters than the respective A-type ones. These observed trends differ from those recently reported by Feng et al., which were obtained on SBA-15 materials templated by preformed lyotropic hexagonal liquid crystal phases at high surfactant concentrations (>20 wt %), without precipitation.[11]

In our experimental conditions (low surfactant concentration, <4 wt %), SBA-15 materials form by precipitation. The mesomorphic order proceeds from the cooperative self-assembly of inorganic precursors with the amphiphilic block copolymers.[7,8] At low pH, protonated PEO chains are associated with silica cationic molecular species through weak electrostatic

Table 5. Values of the Different Structural Parameters Obtained from the Two Models Involving a Corona (Figure 6c,d) for All the Solids of the Series[a]

		A type		B type	
		calcined	uncalcined	calcined	uncalcined
P103					
	r_{BJH} (nm)	1.9		2.5	
uniform	*a* (nm)	8.80	11.00	10.45	10.85
corona	r_1 (nm)	2.2	1.6	3.3	3.3
	r_2 (nm)	3.3	3.7	4.6	4.6
	d_2/d_3	0.43		0.49	
	$(d_2 - d_1)/(d_3 - d_1)$		0.17		0.46
increasing	r_1 (nm)	1.9	2.8	2.9	2.9
density corona	r_2 (nm)	3.8	4.4	5.2	5.1
P123					
	r_{BJH} (nm)	2		3	
uniform	*a* (nm)	9.60	11.85	11.05	11.90
corona	r_1 (nm)	2.5	1.3	3.5	4.1
	r_2 (nm)	3.5	4.0	4.7	5.6
	d_2/d_3	0.33		0.55	
	$(d_2 - d_1)/(d_3 - d_1)$		0.14		0.78
increasing	r_1 (nm)	2.4	3.2	2.9	3.3
density corona	r_2 (nm)	4.0	4.6	5.2	5.4

[a] For comparison, the values of r_{BJH} are also quoted.

interactions mediated by the negatively charged chloride ions. Support for such a mechanism, labeled $S^+X^-I^+$ in the literature,[5,6,40] is obtained by chemical analysis. Indeed, A-type solids have large amounts of chlorine and their Cl/EO molar ratio is close to 1/1 for both P123 and P103. This mechanism explains why, by screening electrostatic repulsive interactions between PEO chains, the inorganic species induce the formation of cylindrical aggregates in a concentration range well below the critical micellization concentration of Pluronics. Figure 8 depicts this organization in which the silica precursors are located within the PEO chains to explain the structure of our AU-type samples.

The transformation of AU-type solids into BU ones is most probably correlated with the fact that the PEO chains become dehydrated with increasing temperature. Recent ESR experiments on another Pluronic (P85) in aqueous solutions at 100 °C have shown that this dehydration may not be uniform.[41] In fact, it is progressive and principally affects the EO groups located in close vicinity of the hydrophobic/hydrophilic interface. In other words, the hydrophilic character increases along

(40) Zhao, D.; Huo, Q.; Feng, J.; Chmelka, B. F.; Stucky, G. D. *J. Am. Chem. Soc.* **1998**, *120*, 6024−6036.
(41) Caragheorgheopol, A.; Caldararu, H.; Dragutan, I.; Joela, H.; Brown, W. *Langmuir* **1997**, *13*, 6912−6921.

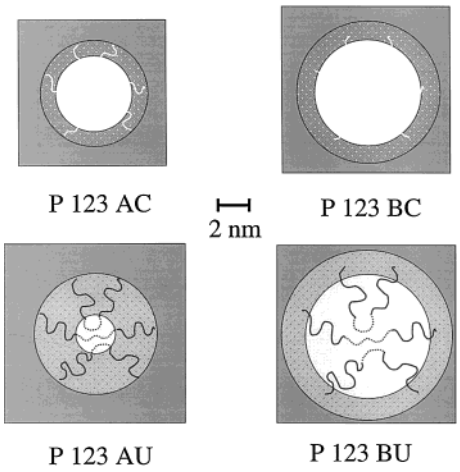

Figure 8. Influence of the hydrothermal treatment on the organization of SBA-15 materials. The shading involves gray levels that correspond to different levels of electron density (in increasing order): pores, PPO cores, corona, dense silica. (All the figures are drawn to scale.)

the PEO chain. If extrapolated in the presence of silica precursors, this behavior would nicely explain the validity of the increasing density corona model and the larger pore sizes detected after calcination. The model depicted in Figure 8 therefore provides insight into the complex structure of SBA-15 materials and into its modification by hydrothermal treatment.

Conclusions

X-ray diffraction quantitative measurements have been performed for the first time on hexagonally ordered mesoporous SBA-15 materials templated by Pluronic triblock copolymers. These measurements cannot be interpreted by considering these solids as ideal arrays of mesopores imbedded in a uniform silica matrix but can be accounted for by models involving a corona, which arises from the partial occlusion of the PEO chains into the silica matrix, and which becomes microporous upon calcination. In this way, quantitative information about pore size, wall thickness, and silica density distribution have been obtained. Moreover, our findings confirm previous ones showing that hydrothermal treatment is a convenient way to tune pore size and wall thickness of SBA-15 materials. In fact, this treatment also deeply modifies the corona by reducing its microporosity.

Acknowledgment. The authors are deeply indebted to Prof. G. Stucky for his constant help and support, to N. Melosh for critical reading of the manuscript, and to M. Lorentz and G. Gonçalves for taking part in this work. The authors also gratefully acknowledge the help of D. Durand (LURE, D43) and M. Gailhanou (LURE, H10) during the synchrotron XRD experiments and thank BASF (Mt Olive, NJ) for donating the block copolymer surfactant Pluronics used in this study.

JA002245H